THREE- DIMENSIONAL NUMERICAL SIMULATION OF BLOOD FLOW IN MOUSE AORTIC ARCH AROUND ATHEROSCLEROTIC PLAQUES

Pauline ASSEMAT[1*], Jillian HOUGH[1], Karen K. SIU[2,3], James A. ARMITAGE[4], Karla G. CONTRERAS[1], Andrea APRICO[5], Karen ANDREWS[5], Anthony DART[5], Jaye CHIN-DUSTING[5] and Kerry HOURIGAN[1]

[1] Department of Mechanical and Aerospace Engineering & Division of Biological Engineering, Monash University, Victoria 3800, AUSTRALIA

[2] Monash Biomedical Imaging, Monash University, Victoria 3800, AUSTRALIA

[3] Australian Synchrotron, 800 Blackburn Rd, Clayton, Victoria 3168, AUSTRALIA

[4] Department of Anatomy and Developmental Biology, Monash University, Victoria 3800, AUSTRALIA

[5] Baker IDI Heart and Diabetes Institute, 75 Commercial Rd, Melbourne, Victoria 3004, AUSTRALIA

*Corresponding author, E-mail address: Pauline.assemat@monash.edu

ABSTRACT

Atherosclerosis occurs due to the build-up and infiltration of lipid streaks in artery walls leading to plaques. Understanding the development of atherosclerosis and plaque vulnerability is of critical importance since plaque rupture can result in heart attack or stroke. Plaques can be divided into two distinct types: those that rupture (vulnerable) and those that are less likely to rupture (stable). In the last decade, researchers have been interested in studying the influence of the mechanical effects (blood shear stress, pressure forces and structural stress) on the plaque formation and rupture processes.

In the literature, physiological experimental studies are limited by the complexity of *in vivo* experiments to study such effects whereas the numerical approach often uses simplified models compared with realistic conditions so that no general agreement of the mechanisms responsible for plaque formation has yet been found. The purpose of the present work is to include more realistic conditions for the calculations of the mechanical effects by implementing real geometries in our numerical model. To this aim, computational fluid dynamics software is used to simulate blood velocity and pressure fields in mice aortic arch.

NOMENCLATURE

Re   Reynolds number
WSS   wall shear stress
WSSG   wall shear stress gradient
OSI   oscillatory shear index

Greek Symbols
ρ density
μ dynamic viscosity
μ-CT   micro-computed tomography

INTRODUCTION

Atherosclerosis is an inflammatory disease characterized by lipid accumulation underneath the endothelium at the boundary of blood vessel walls. In addition to lipid deposition, atherosclerotic progression involves a complex process of monocyte infiltration, lipid oxidation, foam cell formation, smooth muscle cell migration and extracellular matrix production (Chatzizisis et al., 2007, Pello et al., 2011). The lipid core is separated from the circulating blood by a fibrous cap composed of smooth muscle cells and extracellular matrix (Chatzizisis et al., 2007). As plaques develop they can cause luminal narrowing (reduction of the volume of the fluid part), or may undergo expansive remodelling to maintain lumen diameter (Stone et al., 2007). Vulnerable plaques are prone to rupture, with disruption of the fibrous cap exposing the thrombogenic plaque core to the circulating blood (Reininger et al., 2010). Interactions between platelets and the lipid core can induce thrombus formation on the plaque surface, with possible consequences including vessel occlusion, myocardial infarction or stroke. While it is accepted that plaque vulnerability is influenced by fibrous cap thickness and the size of the lipid core (Avgerinos et al., 2011), it also depends on luminal remodelling and hemodynamic parameters for which no general agreement has been found.

Atherosclerotic plaques are found at particular sites in the arterial tree, with plaques commonly found on the inner curvatures of arteries and near bifurcations. This regional localization of atherosclerosis depends largely on hemodynamic factors such as wall shear stress WSS (Chatzizisis et al., 2007). The distribution of hemodynamic field depends on the geometry patterns of the arteries, with low WSS (uni-directional WSS with a low time-average) commonly observed on inner curvatures of arteries and oscillatory WSS (bi-directional WSS with a low time-average) in regions of bifurcations (Cheng et al., 2006). This low WSS hypothesis for plaque formation and progression has been proposed by numerous groups (Gibson et al., 1993, Stone et al., 2007) and has been related to the alteration of cholesterol transport (Caro et al., 1971), up-regulation of the adhesion of molecules that attract leukocytes and of growth factors that promote smooth muscle cells to proliferate and migrate (Chatzizisis et al., 2007) or to the permeability of the endothelial layer (Stangeby et al., 2002). Other hemodynamic factors are also thought to play a role in plaque development including the oscillatory shear index (OSI), which quantifies the temporal variation in WSS, and the wall shear stress gradient (WSSG) corresponding to spatial

WSS variation. Using a laser Doppler velocimetry method, Huo et al. (2008) showed that while the plaques grow in regions of low WSS, atherosclerosis development is enhanced by oscillations in WSS. In an *in vivo* study in mouse carotid arteries, stable plaques were shown to develop in regions of oscillatory WSS and vulnerable plaques in regions of low WSS (Cheng et al., 2006).

In addition, DePaola et al. (1992) showed that large WSSG can induce morphological and functional changes in the endothelium near flow reattachment sites. In addition to these parameters indicating the influence of the viscous forces, pressure forces seem also to affect plaque formation. In their recent paper, Michell et al. (2011) showed that an increase in the vessel internal pressure increases the leukocyte adhesion to the endothelial layer and then enhances one of the biological processes responsible for plaque formation.

Thus, while it is largely agreed that atherosclerotic development occurs in regions of disturbed flow, the exact contributions of various hemodynamic parameters such as WSS, OSI, WSSG and pressure are still under debate.

The present paper will focus on plaque formation by investigating the hemodynamics of blood flow through the mouse aortic arch with and without plaques. The aims of the present paper are: to validate a new numerical approach which not only allows us to take into account the plaques but which will also be directly adaptable as fluid structure interaction code; and to provide some insights into the relation between hemodynamic parameters and plaque development. Three mouse models are being studied: results from wild type C57/B6 mice (no plaque) and ApoE deficient mice (stable plaques) will be presented here. Experiments on a third model, the SM22α-hDTR ApoE deficient mice (vulnerable plaques), are currently under study and will not be presented in this paper. After the tissues have been fixed, the samples are imaged by micro-computed tomography using synchrotron X-ray beams; the resulting images are reconstructed to get the 3D geometries used for the numerical simulations. The originality of our approach consists in removing numerically the plaques to study the plaque formation and development processes on effectively the same aorta. The precise density contrast obtained by Synchrotron imaging enables us to differentiate the plaque from the artery wall.
A high definition is clearly observed for each tissue which can be reconstructed separately using segmentation tools.
In addition, taking into account the complete real geometry will allow us to study the link between the topography of the plaques and their rupture sites. This work is the first step towards a more complex undertaking where it is planned that fluid structure interactions will be taken into account. After the description of the experimental and numerical approach, validation and results will be presented.

MODEL DESCRIPTION

Animal preparation
Animal models provide a key insight to understand atherosclerosis formation. In this study, the Apolipoprotein E knockout (ApoE -/-) mouse model fed a high fat diet (21% fat; 0.15% cholesterol) is used as a model for spontaneous atherosclerotic development (Bond and Jackson, 2011). In the near future, the SM22α-hDTR ApoE-/- will be used as a model which develops vulnerable plaques. Normal mice do not develop atherosclerosis and are used as controls in this investigation. Mice were given a terminal dose of anaesthetic and then transcardially perfused with heparinised saline to clear blood from the vasculature. Tissue was then perfusion fixed with Karnovsky's fluid (2% glutaraldehyde + 4% paraformaldehyde in 0.1M phosphate buffer, pH 7.4). This procedure preserves vessel morphology in the native orientation. Tissues were then dissected, dehydrated through graded butanol and embedded in paraffin.

Imaging

Imaging of the mouse aortas has been obtained by micro-computed tomography (μ-CT) using synchrotron X-ray beams (PSI, Swiss Light Synchrotron, Switzerland) and then reconstructed to derive the 3D geometries used for the numerical simulations (figure 1). The μ-CT data are acquired using monochromatic X-rays of 15keV, and a CCD detector with X-ray converter and interchangeable objective lenses to achieve pixel sizes in the range 2-6 μm (as dictated by the sample size).The samples are imaged using a propagation distance (~2-10cm) to enhance the contrast of the lipid core/fibrous cap. The reconstruction employs the Paganin algorithm (Paganin et al., 2002) using X-TRACT software developed at the CSIRO (Gureyev et al., 2011 http://www.ts-imaging.net/Services/AppInfo/X-TRACT.aspx).
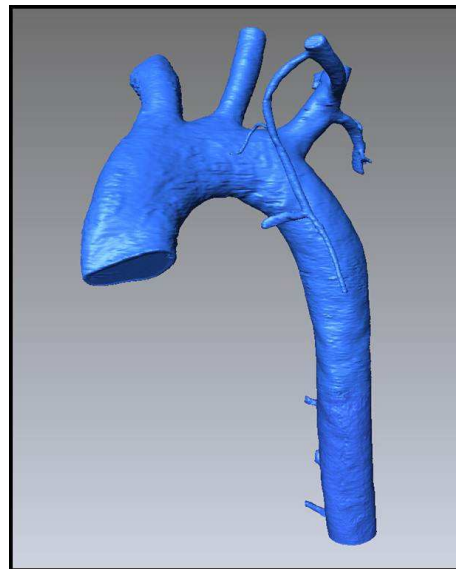

Figure 1: Reconstructed mouse aortic arch.

Numerical methods

Geometry

The software X-TRACT provides two dimensional section images of the geometry which are then reconstructed in the 3D segmentation software AVIZO. The high spatial resolution of the images obtained by μ-CT and the fine density contrast allowed us to differentiate the plaques from the artery walls. An example of an obtained geometry can be seen in figure 2. To verify that the plaques were well defined in AVIZO, histochemical analyses were performed withMasson's Trichrome. Figures 3a and 3b

show, respectively, a section of reconstructed μ-CT image and the associated histology data. On figure 3b, the blue colour corresponds to collagen, the pink colour corresponds to the cytoplasm that characterises the presence of cells. On the right, foam cells which are characteristic of the early stage of plaque formation are visible whereas on the left, the collagen present in the fibrous cap is observed.
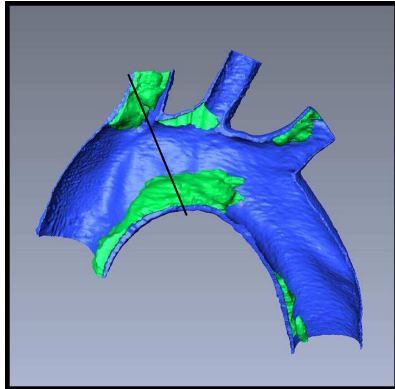

Figure 2: Half aortic arch, coloured blue corresponds to the artery wall, and atherosclerotic plaque coloured green. The black line corresponds to the section plane represented on figure 3.

(a)

(b)
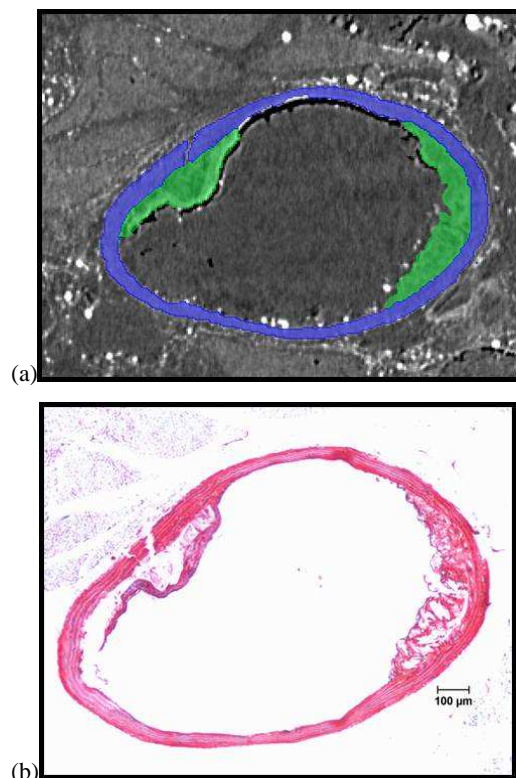
Figure 3: Sections of the three-dimensional geometry located by the line figure 2. (a) Image obtained by μ-CT, the blue colour corresponds to the artery wall, the green to the plaque. (b) Histological analyse of the aortic arch. Sections were cut at 5 μm through the entire aorta and stained with Masson's Trichrome in order to visualise the vascular structures and plaque.

Mesh

The geometry is imported in ICEM CFD to generate the mesh. In the following, only the fluid compartment (lumen) will be considered. The ends of the vessels are extended to prevent boundary condition interactions in the aortic arch zone. Two methods have been tested: tetrahedral and hexahedral meshing. The first type of element is easier to implement but requires a lot of memory for the calculations. Blocking and O-grid methods are used to generate the mesh with hexahedral elements. These methods allow us to control with precision the mesh density and topology, in particular, the size and number of the boundary layers along the geometry can be controlled. In addition, this approach has been shown to tolerate large deformation in a straight vessel model in a study under progress. This not the case for the tetrahedral approach. An example of a hexahedral mesh is given in figure 4. A comparison between these two approaches will be presented in the results section, however the implementation of the hexahedral mesh is under progress and the remaining results are obtained by tetrahedral methods.
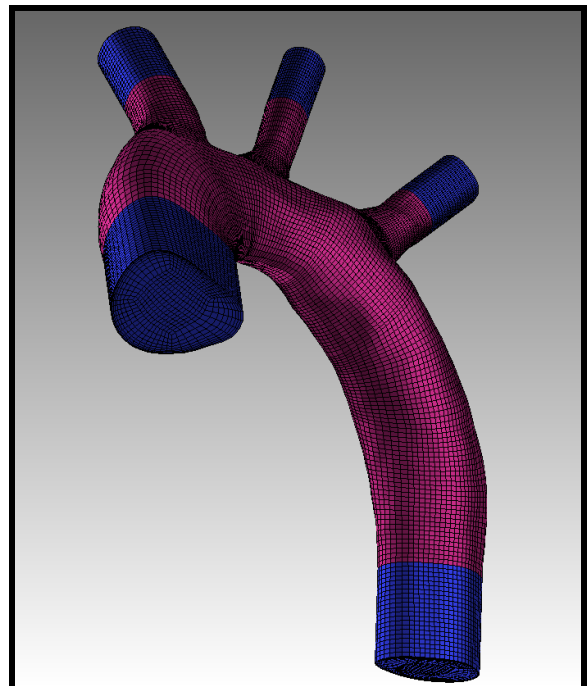
Figure 4: Example of hexahedral mesh designed for a mouse aortic arch without plaque. The pink colour corresponds to the geometry obtained by μ-CT whereas the blue corresponds to extensions.

Numerical model

The Navier-Stokes equations are solved using the element based finite volume methods software ANSYS CFX. A pseudo time-stepping technique method is used to calculate the steady flow. The blood is considered Newtonian as the shear rates calculated are greater than $150s^{-1}$, a condition that makes the Newtonian approximation relatively accurate (Wells et al., 1961). The density ρ and the dynamic viscosity μ are, respectively, $\rho=1060kg/m^3$ and $\mu= 0.0035Pa.s$ (Trachet et al., 2009). Mass flow rate boundary conditions have been applied at

the inlet and the outlet. No-slip boundary conditions have been applied along the rigid walls.

RESULTS

The flow rates used as boundary conditions were obtained from Huo et al. (2008) in which the flow is measured experimentally in the same wild type mice used for the present study. In the following, steady flow is considered to validate our approach. Figure 5 gives the nomenclature for each artery branch, table 1 indicates the flow rates, the diameters and Reynolds from Huo et al. (2008) as well as the measured diameters and calculated Reynolds numbers for the present study.
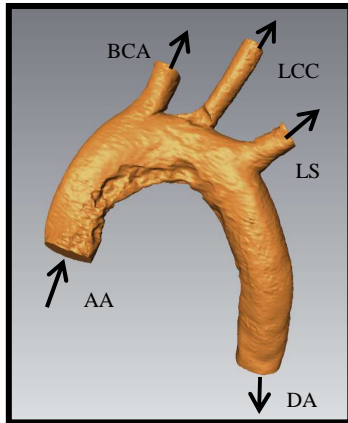

Figure 5: Lumen distribution of a mouse aortic arch with plaques. The inlet and outlets are labelled according to the notations used in table 1.

The Reynolds number is calculated from the equivalent diameter obtained from the measurement of the surface area. In table 1, it is observed that the diameters are smaller than the ones measured by Huo et al. (2008), a difference which probably comes from the difference in the tissue fixing method but also due to the different perfusion pressure. In current experiments, agarose is used as an embedding medium to prevent shrinkage effects caused by paraffin.

As mentioned previously, the first step of the validation is to show invariance of computed parameter magnitudes which are derived from different types of meshes. Figure 5 shows the iso-contours of the WSS for tetrahedral (Figure 6a) and hexahedral (Figure 6b) meshes in rescaled geometries. This scaling implies that the equivalent diameter of the ascending aorta is equal to the one measured in Huo et al. (2008). The maximum of WSS in both configurations are respectively 18.38 and 18.85 Pa for the two different meshes. The difference between these two values is mainly due to the weak control of the boundary layers in the tetrahedral mesh for which the number of elements is 2 times bigger than for the hexahedral. A mesh study has been done on meshes to optimize the numerical parameters but will not be presented here. The performance of our hexahedral approach for a complex real geometry is shown here.

|	AA	BCA	LCC	LS	DA
Flow Rate, Q (mL/min) Huo et al. (2008)	12.02	1.87	1.35	1.06	7.74
Diameter, D (mm) Huo et al. (2008)	1.3	0.85	0.64	0.64	-
Re, Huo et al. (2008)	61	14	14	11	-
Experimental Diameter (mm)	0.84	0.56	0.33	0.38	0.82
Experimental Re	93	22	26	17	60
Scaled Diameters(mm)	1.3	0.68	0.31	0.51	1.08

Table 1: Comparison of diameter and Reynold's number from experimental findings and the values stated in Huo et al. (2008). The experimental dimensions of the aorta and its main branches were measured from the reconstructed three-dimensional geometry. The flow rates used as boundary conditions were obtained from Huo et al (2008). For the fifth row, Re=ρQD/(Aμ) where Q is the flow rate, A is the surface area and D is the equivalent diameter. The discrepancy between the dimensions comes from the shrinkage caused by embedding in paraffin. The last row corresponds to scaled diameters with Huo et al. (2008).
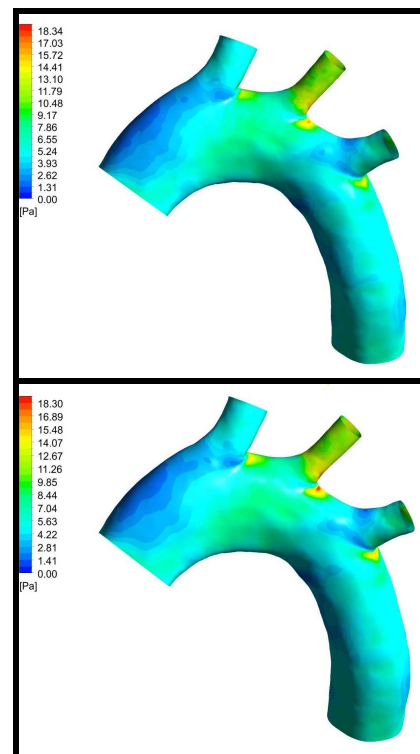
Figure 6: Iso-contours of WSS, (a) tetrahedral mesh, (b) hexahedral mesh.

Consistent with the literature (Huo et al., 2008, Trachet et al., 2009), we find that the local minimum of wall shear stress occurs before the bifurcation (figure 7a) and in the inner curvature of the aortic arch (figure 8a). Qualitatively the iso-contours of WSS have a similar distribution except for the second bifurcation where our geometry presents specificities that make the WSS locally high (small equivalent diameter of this branch). In addition, differences arise from the fact that in both articles, the authors use skeletonisation methods which smooth the geometry and give axisymmetric configurations that do not take into account stenotic plaques. To finish, both cited papers report results for time-averaged WSS. A parallel study (not presented here), taking into account realistic pulsatile flow conditions, showed that the distribution of the WSS on the systole peak is similar to the time averaged WSS itself similar to the results presented in figures 6-8. A quantitative comparison with the previous reference studies will be communicated in the future.
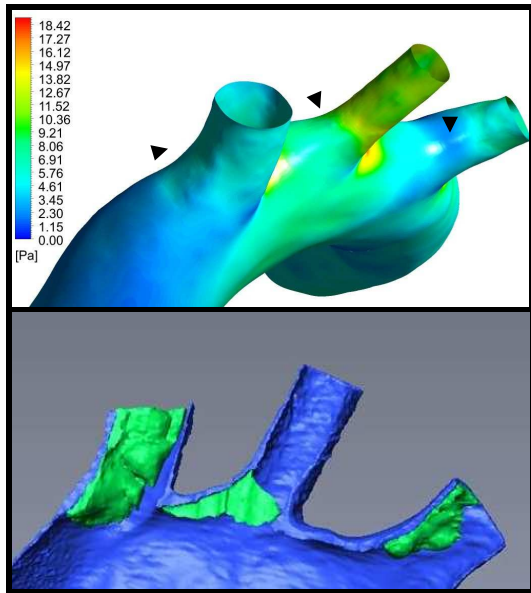

Figure 7: (a) Isocontours of WSS in a geometry without plaque, zoom on the bifurcations, (b) zoom of figure 2.

Figures 7a and 7b, 8a and 8b illustrate that plaques develop around the local minima of wall shear stress and their expansion seems to be directed through the zone where the wall shear stress increases or decreases the least (small gradient of WSS). This observation indicates that the amplitude of WSS is not only important for the formation process but also for the plaque development and lumen remodelling. In addition, it suggests that the assumption of plaques development downstream (Olgac et al. 2009) may be limited, more specifically in complex geometries such as aortic arches. Figure 9 shows the WSS in a geometry where plaques have been considered. A local increase of WSS is observed (indicated by arrows) on all plaques due to the constrictive remodelling of the vessel. A number of studies (Groen et al. 2008, Tang et al. 2009), report a link between high WSS and plaque rupture, however structural stresses are thought to play a more important role (Sadat et al., 2010) in this process. Further investigations with the implementation of fluid-structure interaction is required to resolve this question under debate.
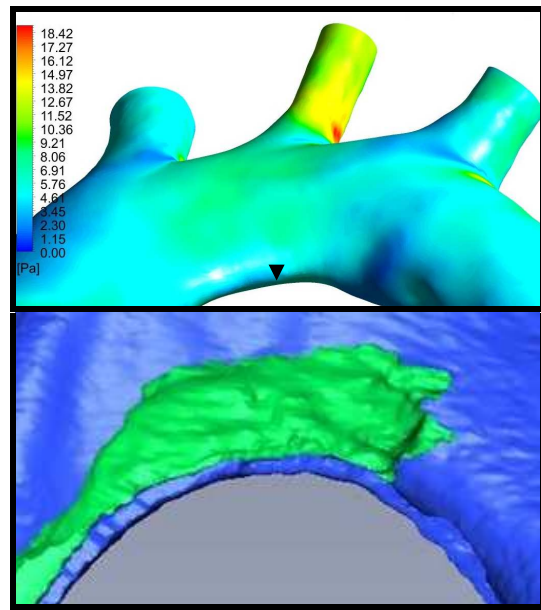
Figure 8: (a) Isocontours of WSS in a geometry without plaque, zoom on the inner curvature, (b) zoom of figure 2.
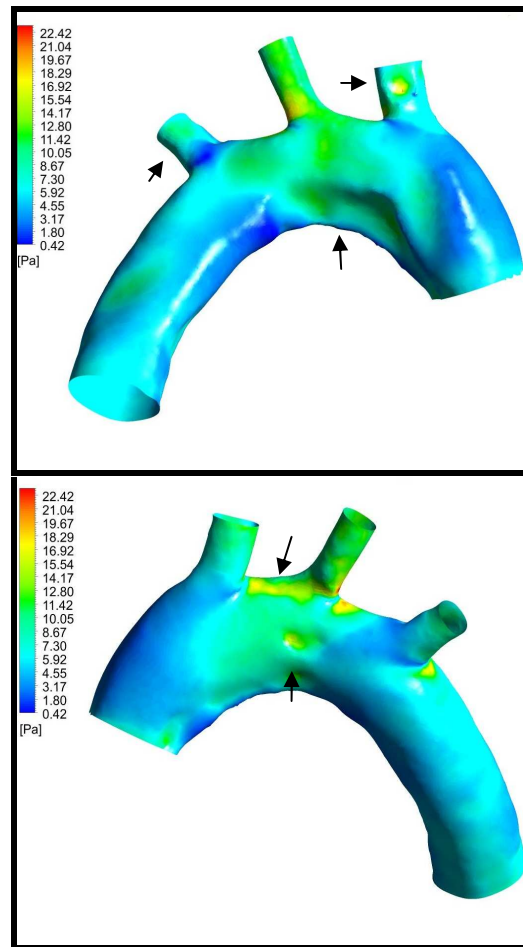
Figure 9: Isocontours of wall shear stress around plaques.

CONCLUSION

This study is a first step in understanding the effect of hemodynamic parameters on plaque formation and development under realistic conditions.

In this article, we have successfully applied an approach that permits the calculation of the blood flow in complex real artery geometries in the presence of plaques. The method of removing the plaque numerically to study the formation and the development of the plaque in the same artery predicts correctly the formation sites around local minimum wall shear stress. In addition, we report that plaque development appears to be in the direction of the smallest gradient of wall shear stress, not only downstream the formation sites as suggested in the literature.

ACKNOWLEDGEMENTS

REFERENCES

AVGERINOS, E.D., GIANNAKOPOULOS, T.G., KADOGLOU, N.P., LIAPIS, C.D., MOULAKAKIS, K.G. and PAPAPETROU, A., (2011), "Biomarkers for diagnosis of the vulnerable atherosclerotic plaque.", *Interventional Cardiology*, **3**(2),223.

BOND, A.R and C. L. JACKSON, (2011), "The fat-fed Apolipoprotein E Knockout mouse brachiocephalic artery in the study of atherosclerotic plaque rupture.", *J. Biomed. Biotechnol*, **2011**, 379069.

CARO, C.G., FITZ-GERALD, J.M. and SCHROTER, R.C., (1971), "Atheroma and Arterial wall shear. Observation, correlation and proposal of a shear dependent mass transfer mechanism for atherogenesis.", *P. R. Soc. London,* **177**(1046), 109-133.

CHATZIZISIS, Y.S., COSKUN, A.U., JONAS, M., EDELMAN, E.R., FELDMAN, C.L. and STONE, P.H., (2007), "Role of endothelial shear stress in the natural history of coronary atherosclerosis and vascular remodelling: molecular, cellular, and vascular behaviour." *J. Am. Coll. Cardiol.*, **49**(25), 2379-2393.

CHENG, C., TEMPEL, D., VAN HAPEREN, R., VAN DER BANN, A., GROSVELD, F., DAEMEN M.J., KRAMS, R. and DE CROM R., (2006), "Atherosclerotic lesion size and vulnerability are determined by patterns of fluid shear stress.", *J. Am. Heart Assoc.*, **113**, 2744-2753.

DEPAOLA, N., GIMBORNE, MA., DAVIS, J.F., and DEWEY, F., (1991), "Vascular endothelium responds to fluid shear stress gradients". *Atherosclerosis and Thrombosis*, **12**, 1254-1257.

GIBSON, C.M., DIAZ, L., KANDARPA, K., SACKS, F.M., PASTERNAK, R.C., SANDOR, T., FELDMAN, C. and STONE, P.H., (1993), "Relation of vessel wall shear stress to atherosclerosis progression in human coronary arteries.", *J. Am. Heart Assoc.*, **13**, 210-315.

GROEN, H.C., GIJSEN, F.J.H., VAN DER LUGT, A., HATSUKAMI, T.S., VAN DER STEEN, A.F.W., YUAN , C. and WENTZEL, J.J., (2007), " Plaque Rupture in the Carotid Artery Is Localized at the High Shear Stress Region.", *Stroke*, **38**: 2379-2381.

GUREYEV, T.E, NESTERETS, Y., TERNOVSKI, D., THOMPSON, D., WILKINS, S. W., STEVENSON, A. W., SAKELLARIOU, A. and TAYLOR J.A, (2011), "Toolbox for advanced X-ray image processing," *Proc. SPIE* **8141**, 81410B, 81410B-14.

HUO, Y., GUO, X. and KASSAB, G.S., (2008), "The flow field along the entire length of the mouse aorta and primary branches.", *Ann. Biomed. Eng.*, **36**(5), 685-699.

MICHELL, D. L., ANDREWS, K. L., WOOLLARD, K. J. and CHIN-DUSTING, J. P., (2011), "Imaging leukocyte adhesion to the vascular endothelium at high intraluminal pressure.", *J. Vis. Exp.,* **54**, e3221.

OLGAC, U., POULIKAKOS, D., SAUR, S.C., ALKADHI, H. and KURTCUOGLU, V., (2009), " Patient-specific three-dimensional simulation of LDL accumulation in a human left coronary artery in its healthy and atherosclerotic states.", *Am. J. Physiol. Heart Circ. Physiol.*, **296**,969-982.

PAGANIN. D.P., MAYO, S.C., GUREYEV, T.E., MILLER, P.R. and WILKINS S.W., (2002), "Simultaneous phase and amplitude extraction from a single defocused image of a homogeneous object.", *J. Microscopy,* **206**(1), 33-40.

PELLO, O.M., SILVESTRE, C., PIZZOL, M.D. and ANDRES, V., (2011), "A glimpse on the phenomenon of macrophage polarization during atherosclerosis.", *Immunobiology*, **216**,1172-1176.

REININGER, A.J., BERNLOCHNER, I., PENZ, S.M., RAVANAT, C., SMETHURST, P., FARNDALE R, W., GACHET, C., BRANDL, R. and SIESS, W., (2010), "A 2-Step Mechanism of Arterial Thrombus Formation Induced by Human Atherosclerotic Plaques.", *J. Am. Coll. Cardiol.*, **55**(11), 1147-1158.

SADAT , U., TENG. Z. and GILLARD, J.H., (2010), "Biomechanical structural stresses of atherosclerotic plaques.", *Expert Rev. of Cardiovasc. Therapy*, **8**(10): 1469-1481.

STANGEBY, D.K. and ETHIER, C.R., (2002), "Computational analysis of coupled blood-wall arterial LDL transport.", *T. ASME*, **124,** 1-8.

STONE, P.H., COSKUN, A.U., KINLAY, S., POPMA, J.J., SONKA, M., WAHLE, A., YEGHIAZARIANS, Y., MAYNARD, C., KUNTZ, R.E. and FELDMAN, C.L., (2007), "Regions of low endothelial shear stress are the sites where coronary plaque progresses and vascular remodelling occurs in humans: and in vivo serial study.", *Eur. Heart J.*, **28**,705-710.

TANG, D., TENG, Z., CANTON, G., YANG, C., FERGUSON, M., HUANG, X., ZHENG, J., WOODARD, P.K. and YUAN, C., (2009), "Sites of rupture in human atherosclerotic carotid plaques are associated with high structural stresses: an in vivo mri-based 3d fluid-structure interaction study.", *Stroke*, **40**: 3258-3263.

TRACHET, B., SWILLENS, A., VAN LOO, D., CASTELEYN, C., DE PAEPE, A., LOEYS, B. and SEGERS P., (2009), "The influence of aortic dimensions on calculated wall shear stress in the mouse aortic arch.", *Comput. Method Biomec.,* **12,** 491-499.

WELLS. R.E., MERRIL, J.W. and MERRILL, E.W., (1961), "Shear rate dependence of the viscosity of whole blood and plasma.", *Science*, **133**(3455), 763-764.